DIVISION S-9—SOIL MINERALOGY

Characterization of Iron, Manganese, and Copper Synthetic Hydroxyapatites by Electron Paramagnetic Resonance Spectroscopy

B. Sutter,* T. Wasowicz, T. Howard, L. R. Hossner, and D. W. Ming

ABSTRACT

The incorporation of micronutrients (e.g., Fe, Mn, Cu) into synthetic hydroxyapatite (SHA) is proposed for slow release of these nutrients to crops in NASA's Advanced Life Support (ALS) program for long-duration space missions. Separate Fe^{3+} (Fe-SHA), Mn^{2+} (Mn-SHA), and Cu^{2+} (Cu-SHA) containing SHA materials were synthesized by a precipitation method. Electron paramagnetic resonance (EPR) spectroscopy was used to determine the location of Fe^{3+}, Mn^{2+}, and Cu^{2+} ions in the SHA structure and to identify other Fe^{3+}-, Mn^{2+}-, and Cu^{2+}-containing phases that formed during precipitation. The EPR parameters for Fe^{3+} (g = 4.20 and 8.93) and for Mn^{2+} (g = 2.01, A = 9.4 mT, D = 39.0 mT and E = 10.5 mT) indicated that Fe^{3+} and Mn^{2+} possessed rhombic ion crystal fields within the SHA structure. The Cu^{2+} EPR parameters (g_z = 2.488, A_z = 5.2 mT) indicated that Cu^{2+} was coordinated to more than six oxygens. The rhombic environments of Fe^{3+} and Mn^{2+} along with the unique Cu^{2+} environment suggested that these metals substituted for the 7 or 9 coordinate Ca^{2+} in SHA. The EPR analyses also detected poorly crystalline metal-oxyhydroxides or metal-phosphates associated with SHA. The Fe-, Mn-, and Cu-SHA materials are potential slow release sources of Fe, Mn, and Cu for ALS and terrestrial cropping systems.

PLANTS WILL SUPPLY food and recycle air and water for humans on long duration missions to the Moon and Mars (Averner, 1989; Allen et al., 1995). The ALS Program of the National Aeronautics and Space Administration (NASA) is developing a synthetic substrate that slowly releases essential nutrients for plant growth on these long-duration missions (Ming et al., 1995; Henderson et al., 2000; Steinberg et al., 2000). This synthetic plant growth substrate (which is called zeoponics) is composed of NH_4^+- and K^+-exchanged clinoptilolite (a natural zeolite) and a nutrient (Fe, Mn, Cu, Zn, Mo, B, S, Cl, Mg) containing synthetic hydroxyapatite (SHA) [$Ca_{10}(PO_4)_6(OH)_2$]. Nutrients incorporated into the sparingly soluble SHA structure are expected to be slowly released from SHA at rates suitable for plant growth.

Infrared spectroscopy, nuclear magnetic resonance (NMR) spectroscopy, x-ray diffraction (XRD) analysis, and Rietveld refinement of XRD powder data have provided evidence that Fe, Mn, and Cu substitute for Ca in the synthetic apatite structure (Suitch et al., 1985; Tripathy et al., 1989; Golden and Ming, 1999; Sutter et al., 2002). Another useful technique for examining the substitution of Fe, Mn, and Cu into the SHA structure is EPR spectroscopy. Electron paramagnetic resonance spectroscopy has characterized the bonding and coordination environment of Fe^{3+}, Mn^{2+}, and Cu^{2+} associated with zeolites (Goldfarb et al., 1994; De Vos et al., 1996; Carl and Larsen, 1999), phyllosilicates (Bergaoui et al., 1995; Muller et al., 1995), glasses (Scholz et al., 1996; Stößer et al., 1996; Cozar et al., 1999), ligands (Chaves et al., 1997), and proteins (Peisach and Blumberg, 1974; DeRose et al., 1995; Horton et al., 1998).

Electron paramagnetic resonance spectroscopy of synthetic fluorapatite single crystals and powders indicated that Mn^{2+} mostly occurred in the Ca(1) site (Kasai, 1962; Ohkubo, 1968; Warren, 1970; Warren and Mazelsky, 1974); however, Mn^{2+} substitution into the Ca(2) site has also been shown by EPR (Ohkubo and Mizuno, 1966; Ohkubo, 1968). Electron paramagnetic resonance spectroscopy has shown that Fe^{3+} was "homogeneously dissolved in hydroxyapatite" (Hornung and Engel, 1992), Fe^{3+} "entered into hydroxyapatite crystals" (Kohen et al., 1984), and that Fe^{3+} was adsorbed onto SHA (Meguro and Ikeya, 1992). Misono and Hall (1973) used EPR to examine the oxidizing and reducing environments of Cu^{2+} in SHA and observed two sets of Cu^{2+} parameters (g_z = 2.43, A_z = 9.0 mT and g_z = 2.36, A_z = 12.5 mT) that they attributed to Cu^{2+} in the Ca(1) and Ca(2) sites.

Several EPR parameters are used when discussing EPR results and they include the g, A, D, and E parameters. The g parameter is a measure of the coupling between the unpaired electron's spin angular momentum (S) with its orbital angular momentum (L) (Symons, 1978). The competition between the ligand(s) competing to remove L and the metal to maintain L causes variations in g values for metal-ligand complexes. This allows EPR to be a valuable tool in delineating between different metal-ligand environments.

The unpaired electron interacts (couples) with the nuclear spin (I) to form a $2I + 1$ line hyperfine structure centered on g and spaced with the distance quantified by the hyperfine coupling parameter A. The coupling between the nuclear and electron spins becomes stronger as the A parameter becomes larger. The combination of g and A parameters can be utilized to differentiate between electron environments of Fe^{3+}, Mn^{2+}, and Cu^{2+} ions.

The EPR zero field splitting (ZFS) parameters D and E measure the deviation of the ion crystal field from ideal tetrahedral or octahedral symmetries and they apply to ions with more than one unpaired electron,

B. Sutter, National Research Council, NASA Ames Research Center, Moffett Field, CA 94035; T. Wasowicz, Dep. of Physics and Astronomy, Georgia State Univ., Atlanta, GA 30303; T. Howard, Dep. of Chemistry, Texas A&M Univ., College Station, TX 77843; L.R. Hossner, Dep. of Soil and Crop Sciences, Texas A&M Univ., College Station, TX 77843; D.W. Ming, NASA Johnson Space Center, Houston TX 77058. Received 6 Aug. 2001. *Corresponding author (b-sutter@mail.arc.nasa.gov).

Published in Soil Sci. Soc. Am. J. 66:1359–1366 (2002).

Abbreviations: ALS, Advanced Life Support; EPR, electron paramagnetic resonance; INAA, instrumental neutron activation analysis; NMR, nuclear magnetic resonance; SHA, synthetic hydroxyapatite; XRD, x-ray diffraction; ZFS, zero field splitting.

e.g., low field Fe^{3+} and Mn^{2+}. However, the broad nature of the Fe^{3+} EPR spectra makes determining *D* and *E* difficult (De Vos et al., 1996). Copper(II) has only one unpaired electron; therefore, *D* and *E* do not apply to Cu^{2+}.

The examples above illustrate that information regarding the structural environments of Fe^{3+}, Mn^{2+}, and Cu^{2+} in the Fe-, Mn- and Cu-SHA materials can be obtained from EPR spectroscopy. While EPR has shown that metals can be incorporated into apatite, no EPR analyses have been conducted on synthetic apatite prepared by the method described here. The SHA materials in this study were produced similarly to those in Golden and Ming (1999), who utilized XRD and infrared spectroscopy to confirm substitution of Fe, Mn, and Cu into SHA. However, the SHA materials examined in this study possess a lower concentration range (0.01–2.5 wt.%) of metals than the SHA materials of Golden and Ming (1999) (1.5–5.0 wt.%). The objectives of this research were to use EPR spectroscopy (i) to show that Fe^{3+}, Mn^{2+}, and Cu^{2+} were incorporated into the SHA, (ii) to characterize their structural environments, and (iii) to characterize other associated phases that might have precipitated during SHA synthesis.

MATERIALS AND METHODS

Iron-, Mn-, and Cu-containing synthetic hydroxyapatites were produced by a procedure similar to Golden and Ming (1999). Calcium nitrate monohydrate [$Ca(NO_3)_2{\cdot}H_2O$] (235 g) was dissolved in 420 ml of 20% (v/v) NH_4OH (Solution A) while $(NH_4)_2HPO_4$ (72.2 g) was dissolved in 380 ml of deionized water (Solution B). After the $(NH_4)_2HPO_4$ was completely dissolved, 30 ml of 20% (v/v) NH_4OH was added. Each transition metal reagent (Table 1) was independently dissolved in 100 ml of deionized water and then added to the B solution. Each mixture of the transition metal and B solutions was mixed for 5 min. The metal-B solution was then added to the A solution and mixed by a propeller stirrer for 24 h. After mixing, the precipitate was allowed to age for 48 h. Subsequently, the supernatant was decanted and then washed with 2.5 L of deionized water three times to remove excess NH_4OH and NO_3^-. The washing procedure was repeated three times. After washing, the SHA precipitate was separated from the liquid by filtering through a Whatman #41 filter paper (Whatman Inc., Clifton, NJ). The SHA precipitate was placed into a cold oven and the temperature was raised to 400°C and maintained for 24 h. The Cu0.1- and Mn0.5-SHA materials were mixed for 5 min not 24 h as were the other SHA materials. When referring to these SHA materials collectively, they will be termed metal-SHA. The number associated with each metal-SHA label is the approximate metal concentration (g kg^{-1}) in SHA.

Table 1. Transition metal reagents used in preparation of synthetic hydroxyapatite (SHA) incorporated with metals.

SHA material†	Transition Metal Reagents	Weight Used
		g
Fe12	$Fe(NH_4)_2(SO_4)_2{\cdot}6H_2O$	8.244
Fe25	$Fe(NH_4)_2(SO_4)_2{\cdot}6H_2O$	17.175
Mn0.5	$MnSO_4{\cdot}H_2O$	0.150
Mn3	$MnSO_4{\cdot}H_2O$	0.727
Mn11	$MnSO_4{\cdot}H_2O$	3.557
Cu0.1	$Cu(NO_3)_2{\cdot}2.5H_2O$	0.117
Cu3	$Cu(NO_3)_2{\cdot}2.5H_2O$	1.000
Cu12	$Cu(NO_3)_2{\cdot}2.5H_2O$	4.880

† Numbers associated with each SHA material indicate their metal concentration (g kg^{-1}).

Total Ca, P, S, Fe, Mn, and Cu analyses were performed with a Cameca SX-50 electron microprobe (Cameca Instrument Inc., Trumball, CT). The SHA materials were pressed into pellets (103.5 MPa) and analyzed at 15 kV and 10 nA with a beam diameter of 20 μm. The electron microprobe sample stage was moved back and forth at 20-m steps over a length of 200 μm to obtain an average chemical analysis. Smithsonian and C.M. Taylor (Gold Beach, OR) polished standards were used to calibrate the electron microprobe.

Instrumental neutron activation analysis (INAA) was performed following a procedure outlined by Golden and Ming (1999) to examine the low concentrations of Mn and Cu in Mn0.5- and Cu0.1-SHA. Samples were encapsulated in pure SiO_2 glass tubes and irradiated at the Texas A&M University nuclear reactor facility for 2 h at a neutron flux of 2.8×10^{12} n cm^{-2} s^{-1}. Counts were performed at 2 h for Mn and 12 h for Cu. Copper data were corrected for interference from positrons produced by pair production from ^{24}Na gamma rays using data from Cu-free samples. Positrons from pair production from other nuclides were insignificant relative to the positrons for ^{64}Cu. The INAA data reduction procedure has been described by Mittlefehldt and Lindstrom (1993), and references therein.

Diethylene-triamine-penta-acetic acid (DTPA) complexes with soluble and exchangeable Fe, Mn, and Cu and mobilizes these metals from Fe-, Mn-, and Cu-containing solid phases (e.g., metal-oxyhydroxides) (Loeppert and Inskeep, 1996). To determine if any nonstructural transition metal phases contributed to the EPR signal, each metal-SHA (0.2 g) was treated with 75 ml of 0.001 *M* DTPA for 24 h on an orbital shaker. After 24 h, the DTPA solution was filtered (0.2-m millipore filter), and fresh DTPA solution was added. This procedure was repeated for a total of three extractions. After the final extraction, the treated metal-SHA materials were dried at 65°C and then examined by EPR along with the untreated metal-SHA materials. After each extraction all solutions were analyzed for Fe, Mn, and Cu using a Perkin Elmer 3100 flame atomic absorption spectrometer (Perkin Elmer, Shelton, CT).

A Bruker ESR 300 (Bruker Biospin Corp., Billerica, MA) was used for X-band (9.43 GHz) EPR at 298 K and 100 K using a variable temperature Oxford Instruments Ltd. liquid nitrogen cryostat (Oxford Instruments Ltd., Santa Clara, CA. A Hewlett Packard HP 5342A frequency counter (Hewlett Packard, Palo Alto, CA) measured the microwave frequency. Iron X-band spectra were collected at 20 mW with modulation amplitude of 2.9 mT. Manganese and Cu X-band spectra were collected at 5 mW with modulation amplitude of 0.5 mT. Q-band (34.0 GHz) spectra were recorded on a Bruker ER200 console and magnet with a Varian E110 Q-band microwave bridge (Varian, Palo Alto, CA) equipped with a tunable TE_{011} Q-band EPR/ENDOR resonance cavity (Sienkiewicz et al., 1996). Copper Q-band spectra were collected using a Janis variable temperature liquid helium cyrostat (Janis Research Company, Inc., Wilmington, MA) at 70 K, 20 mW, and modulation amplitude 0.1 mT. Manganese Q-band spectra were collected at 245 K, 6.3 mW, and modulation amplitude of 0.059 mT. The modulation frequency for all X and Q band EPR analyses was 100 kHz. The Mn0.5-SHA and Cu3-SHA Q- and X-band spectra were simulated with WINEPR SimFonia using second-order perturbation theory, 200 theta angles, and 200 phi angles (Bruker Analytische Messtechnik GmbH, 1996).

Table 2. Total elemental composition of the synthetic hydroxyapatite (SHA) materials along with total amounts of metals extracted by DTPA.

SHA material†	Element						DTPA Extractable‡		
	Ca	P	S	Fe	Mn	Cu	Ext. 1	Ext. 2	Ext. 3
	g kg^{-1}						mg kg^{-1}		
Fe12	362	178	9	12	–	–	4 371	3 242	2 367
Fe25	347	178	9	25	–	–	17 597	2 375	na§
Mn0.5	372	189	nd¶	–	0.5#	–	117	74	83
Mn3	382	182	2	–	3	–	612	354	397
Mn11	366	178	6	–	11	–	4 996	1 752	1 769
Cu0.1	374	190	–	–	–	0.1#	nd¶	nd¶	nd¶
Cu3	380	186	–	–	–	3	987	353	485
Cu12	370	181	–	–	–	12	5 353	1 527	1 641

† Numbers associated with each SHA material indicate their metal concentration (g kg^{-1}).
‡ Each extractable value refers to extracted Fe, Mn, and Cu for the Fe-, Mn-, and Cu-SHA materials, respectively.
§ Data not available.
¶ Below detection limit.
# Instrumental neutron activation analysis.

RESULTS AND DISCUSSION

Total Chemical Analyses and DTPA Extraction

X-ray diffraction confirmed that the metal-SHA materials examined in this study were apatite and that no other crystalline phases were detected (Sutter, 2000). Elemental compositions of metal-SHA are listed in Table 2. The DTPA-extraction data showed that larger amounts of metal were released after the first extraction relative to subsequent extractions (Table 2). The initial high release of metals after the first DTPA extraction suggested the existence of poorly crystalline metal phases along with SHA. This data will be discussed below along with the EPR results, which suggested that Fe^{3+}, Mn^{2+}, and Cu^{2+} were substituted into the SHA structure. The similarity in the amounts of metals released after the second and third DTPA extractions suggested that the metals were from metal-SHA dissolution (Table 2).

Iron Electron Paramagnetic Resonance

Iron(III) possessed distorted octahedral or tetrahedral coordination with rhombic crystal field in Fe12- and Fe25-SHA as indicated by the broad signal composed of a parallel component at $g_{//} = 8.93$ and the well-pronounced perpendicular component centered at $g\perp = 4.20$ (Fig. 1) Goldfarb et al., 1994; Rao et al., 1995; Bordiga et al., 1996; Padlyak and Gutsze, 1998). The high concentration of Fe in both Fe12- and Fe25-SHA did not allow the detection of the ^{57}Fe isotope (natural abundance 2.15%) hyperfine structure. The intensities of the $g_{//} = 8.93$ and $g\perp = 4.20$ peaks for Fe12-SHA did not change significantly after the DTPA treatment, indicating that Fe^{3+} was within the Fe12-SHA structure and inaccessible to DTPA (Fig. 1). The slight decrease of the $g_{//} = 8.93$ indicated that some structural Fe^{3+} leached out of Fe12-SHA (Fig. 1). The Fe25-SHA treated with DTPA had a greater decrease in the $g\perp = 4.20$ and $g_{//} = 8.93$ peak intensities than Fe12-SHA indicating more Fe^{3+} leached out of Fe25-SHA than Fe12-SHA. The higher Fe concentration in Fe25-SHA compared with Fe12-SHA caused more structural instability in Fe25-SHA resulting in a greater loss of structural Fe^{3+} from Fe25-SHA after leaching with DTPA.

Iron-oxyhydroxides within SHA were proposed to have caused the $g\perp = 4.20$ signal; however, that is not possible because iron-oxyhydroxides typically possess signals in the $g = 2.0$ to 2.3 range (Goldfarb et al., 1994; Catana et al., 1995; Lee and Rhee, 1999). The rhombic crystal field symmetry assigned to Fe-SHA suggested that Fe^{3+} was occupying the rhombic Ca(2) site, and not the axial Ca(1) site. However, charge compensation from Fe^{3+} substituting for Ca^{2+} could cause a symmetry distortion and lead to a rhombic environment in the Ca(1) site (E. Solomon, personal communication, 2000). Iron(III) rhombic crystal field symmetry may indicate substitution into either of the Ca sites in SHA. These results are also similar to Kohen et al. (1984) and Hornung and Engel (1992) who concluded that the $g\perp = 4.20$ peak indicated Fe^{3+} was incorporated into their SHA materials.

The broad feature in the $g \cong 2.0$ region has been

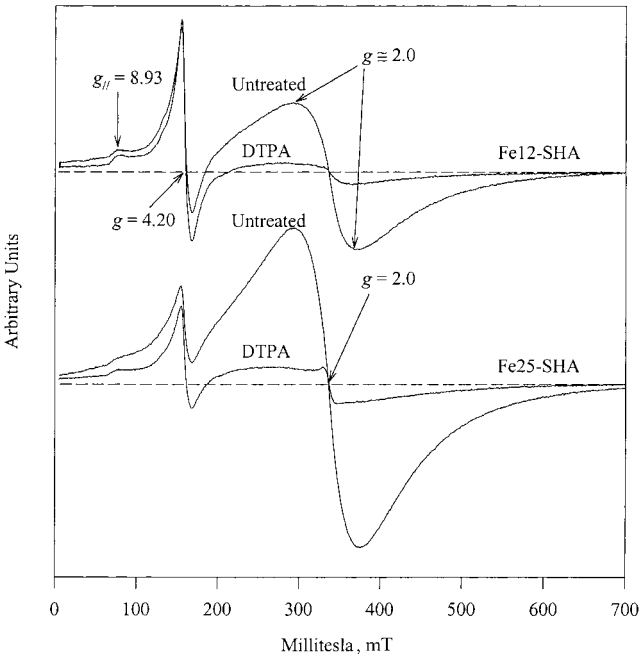

Fig. 1. X-band spectra (298 K) of Fe12-synthetic hydroxyapatite (SHA) and Fe12-SHA treated with DTPA and of Fe25-SHA and Fe25-SHA treated with DTPA. Dashed lines indicates where the derivative of the absorption curve is zero.

attributed to separate ferric oxide phases (Muller et al., 1995), variation of structural Fe^{3+} species with overlapping signals (Catana et al., 1995), surface Fe oxide or oxyhydroxides (Bahranowski et al., 1996), Fe-O-Fe clusters (Stößer et al., 1996), and adsorbed Fe^{3+} on SHA (Meguro and Ikeya, 1992) (Fig. 1). The high concentration of Fe^{3+} associated with SHA caused electron spin-spin interactions between neighboring Fe^{3+} nuclei which yielded the broad $g \cong 2.0$ signal (Ashtekar et al., 1996; Bessergenev et al., 1996; Bogomolova et al., 1996; Bogumil et al., 1993). Spin-spin interaction is caused by small magnetic fields from neighboring paramagnetic ions that alter the total magnetic field of each ion. This caused the energy levels of the unpaired electrons to be shifted (Drago, 1992) which led to a variation of energies resulting in a broadened EPR signal. Poorly crystalline Fe-oxyhydroxides and Fe-phosphates would be expected to have a high concentration of neighboring Fe^{3+} ions. The broadness of the $g \cong 2$ peak supports the existence of poorly crystalline Fe phase(s) associated with Fe-SHA.

The Fe12- and Fe25-SHA treated with DTPA had a lower $g \cong 2.0$ peak intensity relative to the $g \cong 2.0$ peak intensity of Fe12- and Fe25-SHA not treated by DTPA (Fig. 1). The DTPA treatment was not expected to remove large amounts of structural Fe from SHA; hence, the structural Fe^{3+} was not responsible for the large decrease of the $g \cong 2$ peak in samples treated with DTPA. The reduction of the $g \cong 2$ peak with DTPA treatment further suggests that nonstructural poorly crystalline Fe-oxyhydroxides or Fe-phosphates phase(s) were associated with the SHA crystallites. When exposed to DTPA, the poorly crystalline Fe-phase(s) were easily dissolved and removed from the SHA system.

Isolated areas enriched in Fe and P were found associated with SHA as indicated by electron microprobe analysis (data not shown). This suggested that Fe-phosphate may be the cause of the $g = 2$ peak that appeared when the broad $g \cong 2.0$ peak was mostly removed in the Fe25-SHA treated by DTPA (Fig. 1). Sharp $g = 2$ peaks are known to occur with tetrahedral-coordinated Fe^{3+} in $FePO_4$ (Bordiga et al., 1996; Shevade et al., 1997). Kohen et al. (1984) reported that a similar sharp $g = 2$ peak was observed when SHA was exposed to a Fe^{3+} solution, but no explanation was given as to its origin.

Manganese Electron Paramagnetic Resonance

The central $M_s = +1/2 \rightarrow -1/2$ transition (300–360 mT) caused by the Mn^{2+} nuclei ($I = 5/2$) was observed in the Mn0.5- and Mn3-SHA X-band spectra (Fig. 2 and 3). X-band spectra collected at 100 K did not provide any improvement in spectral interpretation; therefore, they were not shown. Manganese(IV) may be the cause of the low field X-band hyperfine patterns (centered on 63, 143, and 214 mT) in Mn0.5- and Mn3-SHA (Fig. 2). Manganese(IV) would have originated from Mn^{2+} oxidation during Mn-SHA synthesis. However, the pink color of the Mn-SHA materials indicated that Mn^{2+} was

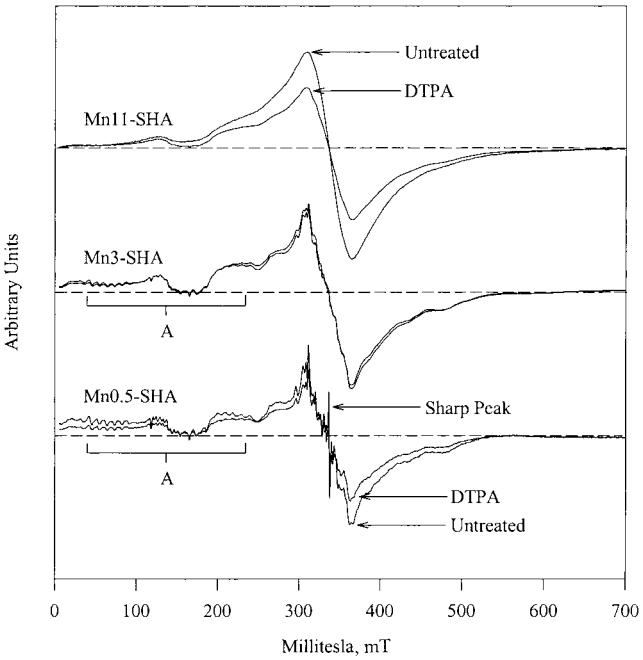

Fig. 2. X-band spectra (298 K) Mn0.5-, Mn3-, and Mn11-synthetic hydroxyapatite (SHA) and Mn0.5-, Mn3-, and Mn11-SHA treated with DTPA. The components of the Mn0.5 and Mn3-SHA spectra marked A indicate a low concentration of another Mn phase. Dashed lines represent where the derivative of the absorption curve is zero. Spectral intensities between samples were scaled for ease of comparison while spectral intensities within samples are similarly scaled. The Mn3-SHA material is not marked DTPA and Untreated because the difference between the DTPA spectra and untreated spectra was difficult to separate.

the dominant oxidation state in the $g = 2$ region of Fig. 2 and 3.

The hyperfine lines of the Mn11-SHA were barely detectable (Fig. 2 and 3). Minor spectral differences were observed between the Mn0.5- and Mn3-SHA and the Mn0.5- and Mn3-SHA treated by DTPA while Mn11-SHA treated by DTPA showed a marked decrease in peak intensity relative to untreated Mn11-SHA (Fig. 2). The large decrease of the Mn11-SHA $g = 2.01$ peak after DTPA treatment indicated that nonstructural Mn phase(s) such as poorly crystalline Mn-oxyhydroxide and Mn-phosphate phase(s) associated with the SHA crystallites were removed by DTPA. Poorly crystalline Mn phase(s) also explain the broad $g = 2.01$ peak in Mn11-SHA that was superimposed on the hyperfine pattern because Mn^{2+} would be closely associated with one another leading to spin-spin interactions (De Vos et al., 1996).

The central sharp peak observed in Mn0.5-SHA was eliminated after DTPA treatment, and was possibly from a small concentration of an inorganic or organic contaminant in the synthesis reagents that was removed by DTPA (Fig. 2 and 3). The high intensity of the Mn^{2+} peaks in Mn3- and Mn11-SHA dominated the spectrum and masked any contamination peak.

Despite the decrease in peak resolution of the X-band hyperfine pattern with increasing Mn concentration, similar Mn spectra were obtained for all Mn concentrations (Fig. 3). This suggested that Mn was occurring in similar structural environment(s) for all Mn-SHA

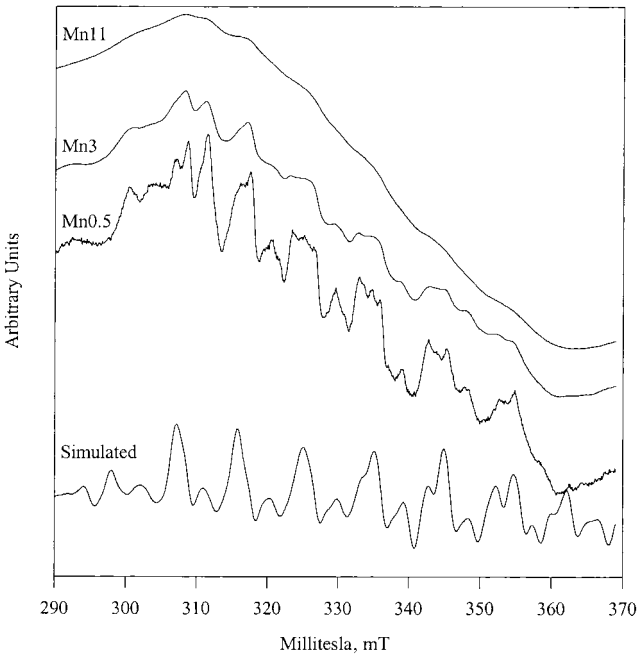

Fig. 3. X-band spectra (298K) of Mn0.5-, Mn3-, and Mn11-synthetic hydroxyapatite (SHA) that were all treated with DTPA. The Mn0.5-SHA simulated spectrum is also presented. Spectral intensities were scaled for ease of comparison.

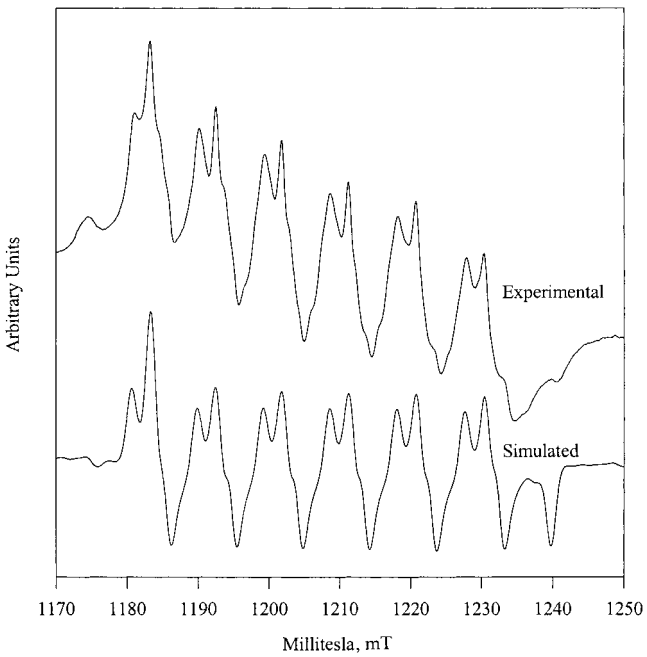

Fig. 4. Q-band spectra (245K) of Mn0.5-synthetic hydroxyapatite (SHA) along with its corresponding simulated spectra.

materials. The occurrence of multiple peaks suggested that more than one Mn^{2+} environment existed in the SHA structure. The X-band spectra were analogous to Mn^{2+} X-band spectra in which Mn^{2+} had rhombic crystal field symmetry in Mn^{2+}-containing Xyl-isomerase (Bogumil et al., 1993).

Q-band EPR improved the quality of the Mn0.5-SHA spectrum by providing a well-resolved six-line hyperfine pattern ($2I + 1$) with double peaks caused by one Mn^{2+} nuclei ($I = 5/2$) (Fig. 4). Q-band EPR utilizes higher magnetic field and microwave frequency, which reduces ZFS effects on the EPR spectrum and decreases the intensity of forbidden transitions ($\Delta M_I = \pm 1$) leading to higher spectral resolution relative to X-band EPR (Bogumil et al., 1993). The Q-band simulation of one Mn^{2+} nuclei environment in Mn0.5-SHA was similar to the experimental spectrum (Fig. 4). The Q-band simulation of the Mn0.5-SHA treated by DTPA spectrum yielded the following EPR parameters $g = 2.01$; $A = 9.4$ mT; $D = 39.0$ mT and $E = 10.5$ mT with x-, y-, and z-line widths of 1.3 mT. The E/D ratio was 0.27, which indicated that a single Mn^{2+} nuclei had a nearly full rhombic crystal field. High spin Mn^{2+} with a full rhombic crystal field will have an E/D ratio of 1/3. The similarity of the Mn0.5-SHA Q-band spectrum to the Q-band rhombic crystal field spectra of Mn^{2+}-containing Xyl-isomerase further supports one Mn^{2+} nuclei environment in the Mn-SHA (Bogumil et al., 1993). Our EPR parameters were near to EPR parameters ($g = 2.00$, $A = 9.6$ mT, $D = 50.4$ mT, and $E = 11.4$ mT) for Mn^{2+} in the Ca(2) (rhombic symmetry) site in a single crystal apatite (Warren, 1970). Mn0.5-SHA parameters did not have all the same parameters as Mn^{2+} in the Ca(1) site (axial symmetry) of powdered flourapatite ($g = 2.00$, $A = 9.44$ mT, $D = 42.8$ mT and $E = 0$ mT) (Kasai, 1962). Parameters similar to flourapatite were obtained for Mn^{2+} in the Ca(1) site of single crystal natural apatite (Burley, 1964; Ohkubo and Mizuno, 1966; Ohkubo, 1968). Substituting the smaller Mn^{2+} (0.80 Å) for the larger Ca^{2+} (0.99 Å) may cause distortion of the Mn-O bonds in the Ca(1) site and lead to rhombic symmetry. Crystalline Mn-oxyhydroxides would have axial symmetry ($E = 0$); therefore, inclusion of crystalline Mn-oxyhydroxides in Mn-SHA was unlikely. The rhombic symmetry parameters suggested that Mn^{2+} substituted in the Ca(2) site or in a strained Ca(1) site in the Mn0.5-SHA.

X-band simulation parameters were the same as the Q-band parameters except that $E = 10.0$ for the X-band simulation which suggested that the simulated parameters were appropriate for Mn0.5-SHA (Fig. 3). While the X-band simulation was not identical to the experimental spectrum, simulated peak positions did corresponded with the Mn0.5-SHA peak positions. Any differences between the X-band simulated and experimental Mn0.5-SHA spectra could be attributed to the forbidden transitions. Nevertheless, the similarity of the X-band simulated and experimental Mn0.5-SHA spectra indicates that the simulated parameters satisfactorily described the Mn environment of Mn0.5-SHA. The X-band $g = 2.01$ peak intensity did not decrease much in Mn0.5- and Mn3-SHA treated by DTPA which provided further evidence that Mn^{2+} resided in the Mn-SHA structure, and was unavailable to DTPA complexation (Fig. 2).

The similarity of the $g = 2.01$ peak positions for the X-band spectra of the Mn-SHA materials indicated that the EPR parameters derived from the Mn0.5-SHA Q- and X-band spectra could be used to describe the Mn3- and Mn11-SHA materials. This also suggested that Mn^{2+} substituted into one of the Ca sites of Mn3- and Mn11-SHA.

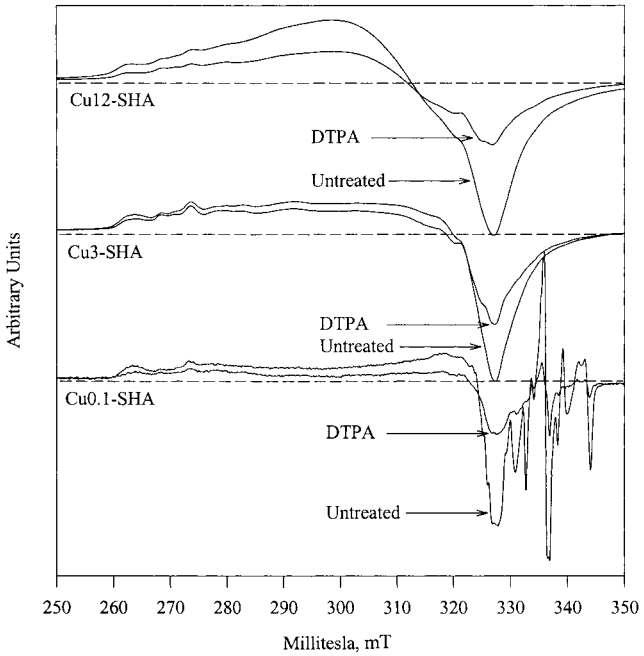

Fig. 5. X-band spectra (100K) of Cu0.1-, Cu3-, and Cu12-synthetic hydroxyapatite (SHA) and Cu0.1-, Cu3-, and Cu12-SHA treated with DTPA. The dashed lines represent where the derivative of the absorption curve equals zero. Spectral intensities between samples were scaled for ease of comparison. Spectral intensities within samples are similarly scaled.

Copper Electron Paramagnetic Resonance

The X-band g_z hyperfine peaks at 100 K had improved peak resolution over the g_z peaks collected at 298 K; therefore, only the 100-K spectra are presented. X-band spectra of the Cu-SHA materials (Fig. 5) and the Cu3-SHA Q-band spectrum (Fig. 6) were similar to spectra

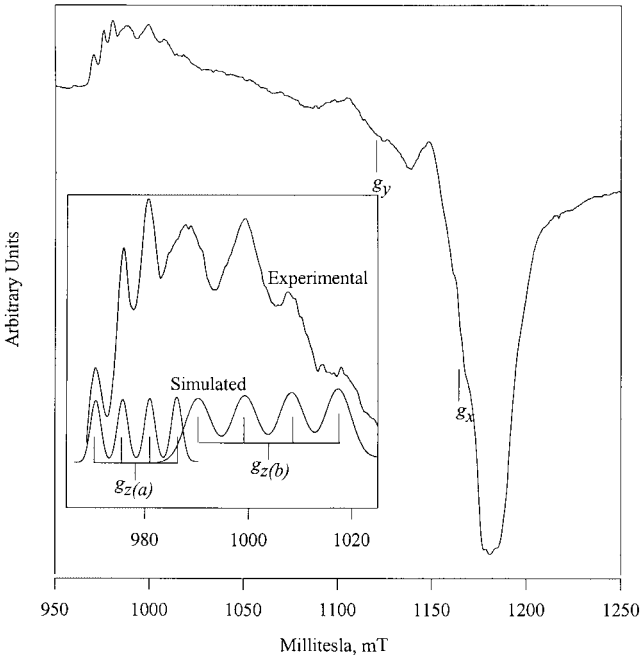

Fig. 6. Q-band spectra (70K) of Cu3-synthetic hydroxyapatite treated with DTPA. Inset graph is expansion of the $g_{z(a)}$ and $g_{z(b)}$ region along with their corresponding simulated spectra.

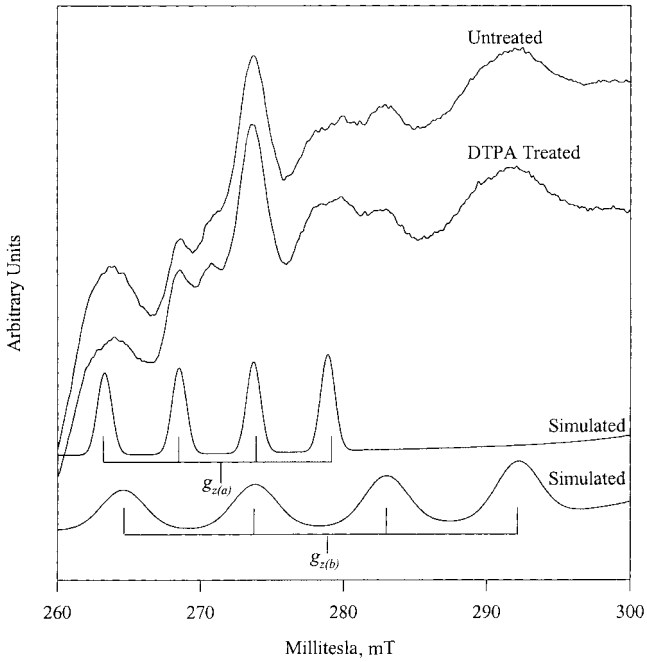

Fig. 7. X-band spectra (100K) of Cu3-synthetic hydroxyapatite (SHA) and Cu3-SHA treated with DTPA. Simulated spectra for the $g_{z(a)}$ and $g_{z(b)}$ regions are presented.

reported in the literature with rhombic spin symmetry ($g_z \neq g_y \neq g_x$) (Reinhammar et al., 1980; Olivia et al., 1997). The interaction of unpaired electrons with the ^{63,65}Cu nuclei (I = 3/2 for both isotopes; 61 and 39% natural abundance, respectively) resulted in the X- and Q-band spectra having g_z regions with a four ($2I$ + 1) peak hyperfine pattern (Fig. 6 and 7).

Spin-spin exchange interactions because of increasing concentrations of Cu^{2+} were the cause of the increased signal broadening as the Cu concentration increased in the Cu-SHA materials (Fig. 5). The entire Cu12-SHA spectrum was superimposed on the broad signal that suggested the presence of sites with strong spin-spin interactions caused by poorly crystalline Cu-oxyhydroxide or Cu-phosphate phase(s). The loss of the spectrum peak intensity with DTPA treatment in the Cu-SHA materials indicated that nonstructural poorly crystalline Cu-oxyhydroxide or Cu-phosphate phase(s) were easily removed from Cu-SHA by DTPA (Fig. 5). The sharp feature between 330 and 345 mT in the Cu0.1-SHA (Fig. 5) greatly decreased with DTPA treatment and was attributed to small amounts of inorganic or organic contamination from the synthesis reagents. The Cu peaks were too intense for the contamination signal to be expressed in Cu3- and Cu12-SHA.

The Q-band simulation of Cu3-SHA yielded $g_{z(a)}$ = 2.488, $g_{z(b)}$ = 2.425, g_y = 2.17, g_x = 2.08 with $A_{z(a)}$ = 5.2 mT, $A_{z(b)}$ = 9.2 mT, and x-, y-, and z-line widths of 2 and 5 mT for $Cu^{2+}_{(a)}$ and $Cu^{2+}_{(b)}$, respectively (Fig. 6). Simulations of the Cu3-SHA X-band spectrum yielded $g_{z(a)}$ = 2.485, $g_{z(b)}$ = 2.420, g_y = 2.17, g_x = 2.08 with $A_{z(a)}$ = 5.2 mT, $A_{z(b)}$ = 9.2 mT, and x-, y-, and z-line widths of 1 and 3 mT for $Cu^{2+}_{(a)}$ and $Cu^{2+}_{(b)}$, respectively (Fig. 7). The X-band parameters were similar to the Q-band parameters indicating that the calculated simulated parameters adequately described Cu3-SHA. The

$g_{z(a)}$ parameters ($g_{z(a)}$ = 2.488; $A_{z(a)}$ = 5.2 mT) were not typical of those found in the literature for Cu-O complexes. Copper bonded to lattice oxygens in montmorillonite $\{[Cu(AlO)_n(H_2O)_{4-n}]^{x+}\}$ possessed g_z parameters no higher than 2.41 to 2.37, and A_z parameters no lower than 10.4 to 14.3 mT (Bahranowski et al., 1996). Similarly, six coordinate Cu^{2+} in physisorbed or frozen $Cu(H_2O)_6^{2+}$ had g_z and A_z parameters that ranged from 2.42 to 2.38 and 11.4 to 13.7 mT, respectively (Duval et al., 1995; Bahranowski et al., 1996; Francois et al., 1997; Schosseler et al., 1997; Carl and Larsen, 1999). Copper(II) substituted into β-$Ca_3(PO_4)_2$ was octahedrally coordinated and had g_z = 2.35 and A_z = 10.24 mT (Romdhane et al., 1981). The change from five-coordinate to six-coordinate Cu-O complexes on zeolite exchange sites has been associated with concomitant increase in $g_{z(a)}$ and decrease in $A_{z(a)}$ parameters (Kucherov et al., 1985; Schoonheydt, 1993; Carl and Larsen, 1999). The higher $g_{z(a)}$ and lower $A_{z(a)}$ parameters relative to six coordinated $Cu(H_2O)_6^{2+}$ and Cu^{2+} in β-$Ca_3(PO_4)_2$ suggested substitution of $Cu^{2+}_{(a)}$ into the seven coordinated Ca(2) site or the nine coordinated Ca(1) site. The decreased intensity of the $g_{z(a)}$ peaks with DTPA treatment suggested that some of the structurally incorporated $Cu^{2+}_{(a)}$ was leached out of SHA (Fig. 7).

The Cu^{2+} $g_{z(b)}$ (2.425) and $A_{z(b)}$ (9.2 mT) parameters were near to six coordinated Cu^{2+} in frozen $Cu(H_2O)_6^{2+}$ and Cu bonded to lattice oxygens in montmorillonite $\{[Cu(AlO)_n(H_2O)_{4-n}]^{x+}\}$ as discussed above. The $g_{z(b)}$ peak intensities were higher than the $g_{z(a)}$ peak intensities before DTPA treatment and had lower peak intensities than $g_{z(a)}$ peak intensities after DTPA treatment (Fig. 7). This indicated that the $Cu^{2+}_{(b)}$ was more readily removed from SHA than $Cu^{2+}_{(a)}$. The Q-band spectra also showed that after DTPA treatment, $g_{z(b)}$ peak intensity decreased more than the $g_{z(a)}$ peaks (data not shown). This observation confirmed the assignment of the g_z and A_z parameters values in the X- and Q-band spectra and suggests that two types of Cu^{2+} ions with different g_z values were present in Cu3-SHA. Furthermore, the $g_{z(b)}$ peaks remained indicating that $Cu^{2+}_{(b)}$ could be crystalline Cu-oxyhydroxide or Cu-phosphate associated with SHA that was partially solubilized by DTPA. Understanding the exact nature of the $Cu^{2+}_{(b)}$ is difficult; however, $Cu^{2+}_{(b)}$ remained after DTPA treatment suggesting that it has potential to serve as a long-term source of Cu^{2+} for plants. The similar peak positions of the g_z, g_y, and g_x regions of the Cu-SHA X-band spectra indicated that the EPR parameters derived from the Cu3-SHA Q- and X-band spectra could be used to describe the Cu0.3 and Cu12-SHA materials.

CONCLUSION

Electron paramagnetic resonance spectroscopy was useful in characterizing the Fe^{3+}, Mn^{2+}, and Cu^{2+} environments in the metal-SHA materials and in the precipitated phases associated with the metal-SHA materials. The EPR spectra suggested that Fe^{3+}, Mn^{2+}, and Cu^{2+} substituted for Ca in SHA. Poorly crystalline metal-oxyhydroxide or metal-phosphate phase(s) were found to be associated with SHA by EPR. Iron phosphate was found associated with the higher Fe containing SHA. The Cu-SHA materials appeared to also possess either a crystalline Cu-oxyhydroxide or a Cu-phosphate component. Recommended future work would utilize a sequential extraction procedure such as that outlined by La Force and Fendorf (2000) coupled with EPR to estimate the extent of the metals present in each phase. The incorporation of Fe, Mn, and Cu into SHA suggests that the metal-SHA materials are promising slow-release sources of micronutrients in the ALS and terrestrial cropping systems.

ACKNOWLEDGMENTS

This research was partially funded by NASA's Graduate Student Researchers Program (NGT51229). The authors would like to thank Ray Guillemette for his assistance with the electron microprobe analysis and Charlie Galindo, Jr for performing the INAA analysis. Special thanks goes to Huay Keng Loke, Matt Vogt, Dan Fraser, and Paul Lindahl for their assistance in EPR analyses and spectral interpretation. The authors gratefully acknowledge Richard Morris for his critical review of this paper.

REFERENCES

Allen, E.R., D.W. Ming, L.R. Hossner, D.L. Henninger, and C. Galindo. 1995. Growth and nutrient uptake of wheat in clinoptilolite-phosphate rock substrates. Agron. J. 87:1052–1059.

Ashtekar, S., S.V.V. Chilukuri, A.M. Prakash, and D.K. Charkrabarty. 1996. Small pore aluminum phosphate molecular sieves with chabazite structure: Incorporation of manganese in the structures -34 and -44. J. Phys. Chem. 100:3665–3670.

Averner, M.M. 1989. Controlled ecological life support system. p. 145–153. *In* D.W. Ming and D.L. Henninger (ed.) Lunar base agriculture: Soils for plant growth. ASA, CSSA, and SSSA, Madison, WI.

Bahranowski, K., R. Dula, M. Labanowska, and E.M. Serwicka. 1996. ESR study of Cu centers supported on Al-, Ti-, and Zr-pillard montmorillonite clays. Appl. Spectrosc. 50:1439–1445.

Bergaoui, L., J.F. Lambert, H. Suquet, and M. Che. 1995. Cu^{II} on Al_{13}-pillard saponites: Macroscopic adsorption measurements and EPR spectra. J. Phys. Chem. 99:2155–2161.

Bessergenev, V.G., V.I. Belyi, A.A. Rastorguev, E.N. Ivanova, Y.A. Kovalevskaya, S.V. Larionov, S.M. Zemskova, V.N. Kirichenko, V.A. Nadolinnyi, and S.A. Gromilov. 1996. Electroluminescent ZnS:Mn films prepared at 220–450°C using complex compounds with sulphur-containing ligands. Thin Solid Films 279:135–139.

Bogomolova, L.D., Y.G. Tepliakov, and F. Caccavale. 1996. EPR of some oxide glasses implanted with Mn^+ and Cu^+ ions. J. Non-Cryst. Solids 194:291–296.

Bogumil, R., R. Kappl, J. Hüttermann, C. Sudfeldt, and H. Witzel. 1993. X- and Q-band EPR studies on the two Mn^{2+}-substituted metal-binding sites of D-xylose isomerase. Eur. J. Biochem. 213: 1185–1192.

Bordiga, S., R. Buzzoni, F. Geobaldo, C. Lamberti, E. Giamello, A. Zecchina, G. Leofanti, G. Petrini, G. Tozzola, and G. Vlaic. 1996. Structure and reactivity of framework and extraframework iron in Fe-silicalite as investigated by spectroscopic and physiochemical methods. J. Catalysis 158:486–501.

Bruker Analytische Messtechnik GmbH. 1996. WINEPR SimFonia shareware. Version 1.25. Bruker Analytische Messtechnik GmbH, Rheinstetten, Germany.

Burley, S.P. 1964. The allowed and forbidden transitions in the paramagnetic resonance of the manganese ion in trigonal sites apatite and smithsonite. Aust. J. Phys. 17:537–542.

Carl, P.J., and S.C. Larsen. 1999. Variable-temperature electron paramagnetic resonance studies of copper-exchange zeolites. J. Catal. 182:208–218.

Catana, G., J. Pelgrims, and R.A. Schoonheydt. 1995. Electron spin resonance study of the incorporation of iron in ferrisilicalite and FAPO-5. Zeolites 15:475–480.

Chaves, S., A. Cerva, and R. Delgado. 1997. Tris(carboxymethyl)oxa-

triazamacrocycles and their metal complexes. J. Chem. Soc. Dalton Trans. 22:4181–4189.
Cozar, O., I. Ardelean, V. Simon, V. Mih, and N. Vedean. 1999. EPR study of phosphate glasses containing two types of transitional metal ions. J. Magn. Magn. Mat. 196–197:269–271.
DeRose, V.J., C.H. Kim, W.E. Newton, D.R. Dean, and B.M. Hoffman. 1995. Electron spin echo envelope modulation spectroscopic analysis of altered nitrogenase MoFe proteins from Azotobacter vinelandii. Biochemistry 34:2809–2814.
De Vos, D.E., B.M. Weckhuysen, and T. Bein. 1996. ESR fine structure of manganese ions in zeolite A detects strong variations of the coordination environment. J. Am. Chem. Soc. 118:9615–9622.
Drago, R.S. 1992. Physical methods for chemists. Saunders and Harcourt Brace Jovanovich, Ft. Worth, TX.
Duval, E., C. Bovier, H. Roux, J. Serughetti, A. Tuel and G. Wicker. 1995. Magnetic properties of Cu-doped porous silica gels study by magnetic resonances. J. Non-Cryst. Solids 189:101–106.
Francois, J., C. Heitz, and M.M. Mestdagh. 1997. Spectroscopic study (u.v.-visible and electron paramagnetic resonance) of the interactions between synthetic polycarboxylates and copper ions. Polymer 38:5321–5332.
Golden, D.C., and D.W. Ming. 1999. Nutrient-substituted hydroxyapatites: Synthesis and characterization. Soil Sci. Soc. Am. J. 63:657–664.
Goldfarb, D., M. Bernardo, K.G. Strohmaier, D.E.W. Vaughan, and H. Thomann. 1994. Characterization of iron in zeolites by X-band and Q-band ESR, Pulsed ESR, and UV-visible spectroscopies. J. Am. Chem. Soc. 116:6344–6353.
Henderson, K.E., D.W. Ming, C. Carrier, J.E. Gruener, C. Galindo, Jr., and D.C. Golden. 2000. Effects of adding nitrifying bacteria, dolomite, and ferrihydrite to zeoponic plant growth substrates. p. 441–447. *In* C. Colella and F.A. Mumpton (ed.) Natural zeolites for the third millennium. De Frede Editore, Naples, Italy.
Hornung, R., and A. Engel. 1992. Preparation and characterization of ivory-coloured hydroxyapatite. J. Mater. Sci. Lett. 11:958–959.
Horton, T.E., R.D. Clardy, and V.J. DeRose. 1998. Electron paramagnetic resonance spectroscopic measurement of Mn^{2+} binding affinities to the hammerhead ribozyme and correlation with cleavage activity. Biochemistry 37:18094–18101.
Kasai, P.H. 1962. Electron paramagnetic resonance study of Mn^{++} ion in polycrystalline calcium fluorophosphate. J. Phys. Chem. 66: 674–680.
Kohen, R., M. Friedman, and M. Chevion. 1984. Iron-treated hydroxyapatite: Structure and function. Pharm. Acta Helv. 59:228–234.
Kucherov, A.V., A.A. Slinkin, D.A. Kondrate'ev, T.N. Bondarenko, A.M. Rubinstein, and K.M. Minachev. 1985. Cu^{2+}-cation location and reactivity in mordenite and ZSM-5-ESR study. Zeolites 5:320–324.
La Force, M.J., and S. Fendorf. 2000. Solid-phase iron characterization during common selective sequential extractions. Soil Sci. Soc. Am. J. 64:1608–1615.
Lee, H.T., and H.K. Rhee. 1999. Stability of Fe/ZSM-5 de-Nox catalyst: effects of iron loading and remaining Brønsted acid sites. Catal. Lett. 61:71–76.
Loeppert, R.H., and W.P. Inskeep. 1996. Iron. p. 639–664. *In* D.L. Sparks (ed.) Methods of soil analysis. Part 3. SSSA Book Series No. 5, SSSA, Madison, WI.
Meguro, K., and M. Ikeya. 1992. Stabilization of radicals by doping from aqueous solutions into crystals of hydroxyapatite. Jpn. J. Appl. Phys. 31:1353–1357.
Ming, D.W., D.J. Barta, D.C. Golden, C. Galindo, Jr., and D.L. Henninger. 1995. Zeoponic plant growth substrates for space applications. p. 505–515. *In* D.W. Ming and F.A. Mumpton (ed.) Natural zeolites '93: Occurrence, properties, use. International Committee on Natural zeolites. Brockport, NY.
Misono, M., and W.K. Hall. 1973. Oxidation-reduction properties of copper- and nickel-substituted hydroxyapatites. J. Phys. Chem. 77: 791–800.
Mittlefehldt, D.W., and M.M. Lindstrom. 1993. Geochemistry and petrology of a suite of ten Yamato HED meteorites. Proc. Natl. Inst. Polar Res. (Japan) Symp. Antarctic Meteorites 6:268–292.
Muller, J.P., A. Manceau, G. Calas, T. Allard, P. Ildefonse, and J.L. Hazemann. 1995. Crystal chemistry of kaolinite and Fe-Mn oxides: Relation with formation conditions of low temperature systems. Am. J. Sci. 295:1115–1155.
Ohkubo, Y. 1968. EPR spectra of Mn^{2+} ions in synthetic calcium fluoro-chloro phosphates. J. Appl. Phys. 39:5344–5345.
Ohkubo, Y., and H. Mizuno. 1966. Electron paramagnetic resonance of Mn^{2+} ions in calcium halophosphates. Proc. Int. Conf. Lumi. 7:1330–1336.
Olivia, C., E. Selli, A. Ponti, L. Correale, V. Solinas, E. Rombi, R. Monaci, and L. Forni. 1997. FTIR and EPR characterization of copper-exchange mordenites and beta zeolites. J. Chem. Soc. Faraday Trans. 93:2603–2608.
Padlyak, B.V., and A. Gutsze. 1998. EPR study of the impurity paramagnetic centres in (CaO-Ga_2O_3-GeO_2) glasses. Appl. Magn. Reson. 14:59–68.
Peisach, J., and W.E. Blumberg. 1974. Structural implications derived from the analysis of electron paramagnetic resonance spectra of natural and artificial copper proteins. Arch. Biochem. Biophys. 165:691–708.
Rao, A.S., R.R. Reddy, T.V.R. Rao, and J.L. Rao. 1995. Electron paramagnetic resonance and optical absorption spectra of Fe^{3+} ions in alkali cadmium borosulphate glasses. Solid State Comm. 96:701–705.
Reinhammar, B., R. Malkin, P. Jensen, B. Karlsson, L.E. Andréasson, R. Aasa, T. Vänngård, and B.G. Malmström. 1980. A new copper(II) electron paramagnetic resonance signal in two laccases and in cytochrome *c* oxidase. J. Bio. Chem. 255:5000–5003.
Romdhane, S.S., G. Bacquet, and G. Bonel. 1981. Etude des phases et haute pression du phosphate tricalcique par la RPE de l'ion Cu^{2+}. (In French.) J. Solid State Chemistry 40:34–41.
Scholz, G., R. Stößer, S. Sebastian, T. Grande, S. Aasland, and M. Nofz. 1996. On the incorporation of copper ions in heavy metal fluoride glasses. Ber. Bunsenges. Phys. Chem. 100:1617–1620.
Schoonheydt, R.A. 1993. Transition-metal ions in zeolites: Siting and energetics of Cu^{2+}. Catal. Rev. Sci. Eng. 35:129–168.
Schosseler, P.M., B. Wehrli, and A. Schwiger. 1997. Complexation of copper(II) with carbonate ligands in aqueous solution: A CW and pulse EPR study. Inorg. Chem. 36:4490–4499.
Shevade, S., R.K. Ahedi, and A.N. Kotasthane. 1997. Synthesis and characterization of ferrisilicate analogs of ferrierite (Fe-FER) zeolites. Cat. Lett. 49:69–75.
Sienkiewicz, A., B.G. Smith, A. Veselov, and C.P. Scholes. 1996. Tunable Q-Band resonator for low temperature electron paramagnetic resonance/electron nuclear double resonance measurements. Rev. Sci. Instrum. 67:2134–2138.
Steinberg, S.L., D.W. Ming, K.E. Henderson, C. Carrier, J.E. Gruener, D.J. Barta, and D.L. Hennninger. 2000. Wheat responses to differences in water and nutrient status between zeoponic and hydroponic growth systems. Agron. J. 92:353–360.
Stößer, R., G. Scholz, M. Nofz, T. Grande, and S. Aasland. 1996. On the nature and role of Fe^{3+} ions in oxide and fluoride glasses. Ber. Bunsenges. Phys. Chem. 100:1588–1592.
Suitch, P.R., J.L. LaCout, A. Hewat, and R.A. Young. 1985. The structural location and role of Mn^{2+} partially substituted for Ca^{2+} in fluorapatite. Acta Crystallogr. B41:173–179.
Sutter, B., R.E. Taylor, L.R. Hossner, and D.W. Ming. 2002. Solid state ^{31}phosphorus nuclear magnetic resonance of iron-, manganese-, and copper-containing synthetic hydroxyapatites. Soil Sci. Soc. Am. J. 66:455–463.
Sutter, B. 2000. Structural properties and dissolution of iron, manganese, and copper containing synthetic hydroxyapatite. Ph.D. diss. Texas A&M University, College Station.
Symons, M. 1978. Chemical & biological aspects of electron-spin resonance spectroscopy. John Wiley & Sons, New York.
Tripathy, N.K., P.N. Patel, and A. Panda. 1989. Preparation, IR, and lattice constant measurments of mixed (Ca + Cu + Zn) hydroxylapatites. J. Solid State Chem. 80:1–5.
Warren, R.W. 1970. EPR of Mn^{+2} in calcium fluorophosphate. I. The Ca(II) site. Phys. Rev. B 2:4383–4388.
Warren, R.W., and R. Mazelsky. 1974. ESR of Mn^{+2} in calcium fluorophosphate. II. Modified Ca(II) sites. Phys. Rev. B 10:19–25.